
Microstructure and Hardness in GTA Welding of Stainless Steel

P. Maran¹, T. Sornakumar² and T. Sundararajan³

¹Lecturer, Department of Mechanical Engineering, Thiagarajar College of Engineering, Madurai-625015, India

²Professor, Department of Mechanical Engineering, Thiagarajar College of Engineering, Madurai-625015, India

³Professor, Department of Mechanical Engineering, Indian Institute of Technology, Madras, Chennai-600036, India

ABSTRACT

The experimental studies on microstructures and micro hardness in the weld metal show that the fluid flow pattern in the weld pool strongly influences the cooling rate, microstructure and hardness. The fluid pattern predicted is correlated with the experimental results for microstructures and hardness. The spatial variations of micro hardness show that the micro hardness values are higher in the low velocity fluid flow region and lower in the remaining region. The variations are due to different cooling rates, micro structures, sizes of the grains and delta ferrite content.

Keywords: Modeling, Weld pool, Fluid flow, Weld bead geometry, Microstructure, Micro hardness.

INTRODUCTION

Welding of material leads to heating, melting, formation of weld pool and weld bead. When the welding torch is held over the material, a small weld pool of molten metal is formed below the welding torch. The molten metal gets solidified when the heat source moves away and produces a weld bead. But, during the short time duration of welding, the molten metal in the weld pool has movement within the pool due to various driving forces such as buoyancy, electromagnetic and surface tension forces. The fluid flow in the weld pool significantly affects the temperature fields, thermal cycles, weld bead geometry, and microstructures. The microstructure in turn affects the properties of the weldment, such as hardness, strength, ductility, toughness and corrosion resistance.

For larger heat input to the metal, the peak temperature and weld pool size get increased. The fluid velocity also increases with increase in heat input and affects the shape of contours for isotherms, the cooling rates and microstructures. This leads to the

changes in the size and shape of the weld pool and the resultant weld bead. The cooling rate and solidification mode are also influenced by the fluid flow pattern. Thus, it is important to understand how the heat and fluid flow in the weld pool influence the microstructure and hardness of the weldment.

Oreper and Szekely [1] developed a 2-D (two-dimensional), axisymmetric, heat and fluid flow model to study the temperature and velocity fields in the Gas Tungsten Arc (GTA) weld pool. Zacharia et al. [2-4] theoretically and experimentally investigated the temperature and velocity fields during spot and linear GTA welding of AISI type 304 stainless steel plates. The effect of variation in the surface tension coefficient with respect to temperature on the fluid flow was studied. Choo et al. [5,6] developed an integrated model of arc and weld pool to study the effect of current on free surface depression. It was observed that the surface depression in excess of 1 mm is found for currents larger than 240 A. Maran et al. [7,8] developed an equivalent 2-D

finite volume heat and fluid flow model to calculate the temperature and velocity fields, weld bead width and penetration in a linear GTA welding.

Iamboliev et al. [9] revealed the mechanism of full austenitic microstructure in the GTA weld metal zone of austenitic stainless steel of type AISI type 310S and 304. Basu and Raman [10] studied the effects of heat input, as a whole, and individual welding parameters such as welding current and speed under isoheat input conditions on the microstructural variations of as deposited weld metal obtained by single pass bead-in-groove submerged arc welding. Inoue et al. [11] studied the relation of microstructure with local hardness of low activation ferritic steel (JLF-1) used for fusion reactor structural components. Norman et al. [12] investigated the weld microstructures of autogenous GTA welds in an Al-Cu-Mg-Mn alloy for a wide range of welding condition. Finest microstructure and high hardness were observed in the weldment at higher cooling rates.

In the present work, a detailed

investigation was carried out on AISI Type 304 stainless steel plates of 4.35 mm thickness during GTA welding to understand the relation between the fluid flow and micro hardness variations in the weld metal zone.

MATHEMATICAL MODELIN

A two dimensional heat and fluid flow model developed has been used to calculate the temperature and velocity fields in the weld pool formed during GTA welding of 4.35 mm thick stainless steel plate. The fluid flow is assumed as laminar and the properties except surface tension and thermal conductivity are considered as independent of temperature. The continuity, momentum and energy equations have been explained by Maran et al. [7,8]. The top, side and bottom surfaces of the plate are exposed to ambient conditions during welding. Heat transfer to the surroundings occurs both by convection and radiation. The surface tension force is balanced by the viscous force on the free surface of the weld pool. The equations for boundary conditions have been explained in earlier literatures [7,8].

In general, in the solid region (with temperature less than the solidus temperature) both velocity components u and v are set to zero at all locations. The release or absorption of latent heat due to phase change at the liquid-solid interface has been considered by accounting for the latent heat in the form of an equivalent enhanced specific heat for the nodes in the phase change region (with temperature between solidus and liquidus temperatures). The bead on plate welding is made on AISI 304 L stainless steel plate of size 80 mm x 80 mm x 4.35 mm. Half of the plate, about the weld symmetry is considered for the computational study. An 80 x 80 grid system has been used in the

calculation. The computation is carried out for the period of arcing duration at each cell, with a time step of 0.0002 s. This period is calculated from beam radius and welding speed [7,8].

The computational domain, a rectangle of size 40 mm x 4.35 mm, is divided into a number of rectangular cells of variable spacing. Finer grids are used nearer to the heat source, whilst further away relatively coarser grids are employed. For the numerical solution of governing equations, the problem domain is covered by a set of rectangular control volumes. The discretization is performed using a staggered grid that consists of temperature / velocity nodes and pressure nodes. The gradient of surface tension with respect to temperature has been assumed as a positive constant equal to 10^{-5} N/m K for temperature less than 2200 K and a negative constant equal to 10^{-5} N/m K for higher temperatures. The arc efficiency (η) is 80 %, the beam radius (r_b) for heat distribution is 0.003 m and the beam radius for current distribution (r_c) is 0.003 m. The properties of material used in the computations are given in Table 1 [7,8].

EXPERIMENTAL WORK

Autogenous bead-on-plate GTA welds were made on 4.35 mm thick, AISI type 304L stainless steel plates with 80 ppm sulphur content. The work material was cut into test pieces of 80 x 80 x 4.35 mm size. Weld beads were laid along the center line of the plate. During welding, the arc gap was maintained at 2 mm and the shielding gas was supplied at 16 liters per minute. The top and side surfaces were exposed to an ambient temperature of 303 K. Welding current and voltage were measured using a digital ammeter and voltmeter, provided in the welding machine. The time taken for welding was measured with a digital stop clock. The welded plates were cut

across the weld bead to get the macroscopic view of the weld bead. The weld bead depth and width have been measured with a micrometer attached with optical microscope. The microstructures were also examined in the weld metal zone and heat affected zone, using an optical microscope. The vickers hardness values in the weld metal and heat affected zone were measured using a micro hardness testing machine at 100 gram load and 15 second loading time. The measurements were taken at every 0.5 mm distance in the x-direction and 0.2 mm in the y-direction.

RESULTS AND DISCUSSION

Table 2 presents the comparison of theoretical and experimental weld bead dimensions for two different welding speeds (5.0 mm/s and 2.66 mm/s) at 120 A and 14 V [7, 8]. The results also show the effect of welding speed on peak temperature, maximum velocity in the weld pool and weld bead dimensions. The peak temperature, half width of weld bead and depth of penetration increase with heat input. The temperature field for the welding conditions of 120 A, and 14 V at a welding speed of 2.66 mm/s are discussed by Maran et al [8]. The weld bead geometry was determined from the isotherm drawn for solidus temperature. The corresponding velocity field showed double loop circulation in the weld pool creating a low velocity region in the center of the loop.

To understand the effect of velocity on the microstructure and hardness, metallographic test and micro hardness survey have been conducted. The micro hardness distribution in the weld metal, measured at certain nodes at regular spacing in the x and y direction has been presented in Table 3. The spatial

variations of micro hardness in the x directions at certain sections in the vertical direction (y), from the top surface have been presented in Fig. 1. All three sections present an almost similar 'W' type curve. It also confirms that the hardness values are relatively smaller in the regions of fluid flow and higher for the regions where flow velocity is negligible. The hardness values for the weld metal zone are lower than that of the heat affected zone and base metal.

Examinations on microstructure have recognized that the welding speed and cooling rates affect the solidification mode. The base metal (Fig. 2) shows the austenite (A) grains. Fig. 3 shows the microstructures in the solid-liquid interface region. The grains are larger in the heat affected zone and finer grains are found in the interface region. Higher hardness has been measured for the region where the grains are smaller in size. Columnar dendrites are seen in the weld interface region. In Fig. 4, the weld metal microstructures reveal predominantly vermicular ferrite and lacy ferrite as well as acicular ferrite in an austenite matrix. The ferrite morphologies are attributed to FA (Ferritic-Austenitic) solidification and F (Ferritic) solidification mode followed by a solid state ferrite to austenite transformation as reported by Iamboliev et al. [9].

CONCLUSIONS

The effects of weld pool convection on cooling rates, micro hardness and microstructure were studied using experimental results and theoretical calculation. The microstructure of the weld metal has delta ferrite in the austenite matrix. The spatial variations of micro hardness across the weldment in various sections in the thickness direction show that the micro hardness values are higher in the low velocity fluid

flow region and lower in the remaining region. The variations are due to different micro structures, cooling rates, size of the grains and delta ferrite formation in austenite matrix in the weld metal.

REFERENCES

1. G.M.Oreper, J.Szekely, Heat and fluid flow phenomena in weld pools, *Journal of Fluid Mechanics*. 147 (1984) 53-79.
2. T. Zacharia, S.A. David., J. M. Vitek, T. DebRoy, Weld pool development during GTA and Laser beam welding of type 304 stainless steel, Part I Theoretical Analysis, *Welding Journal*. 68 (1989) 499-s - 509-s.
3. T.Zacharia, S.A.David., J. M. Vitek, T. DebRoy, Weld pool development during GTA and Laser beam welding of type 304 stainless steel, Part II Experimental Correlation, *Welding Journal*. 68 (1989) 510-s - 519-s.
4. T.Zacharia, S.A.David, J. M. Vitek and H.G. Kraus, Computational modeling of stationary Gas Tungsten Arc Weld pools and comparison to stainless steel 304 experimental results, *Metallurgical Transactions B*. 22B (1991) 243-257.
5. R. T. C. Choo, J. Szekely, R.C.Westhoff, On the calculation of the free surface temperature of gas-tungsten-arc weld pools from first principles: Part I: Modeling the welding arc, *Metallurgical Transactions B*. 23 B (1992) 357369
6. R. T. C. Choo, J. Szekely, R.C.Westhoff, On the calculation of the free surface temperature of gas-tungsten-arc weld pools from first principles: Part II: Modeling the weld pool and comparison with experiments, *Metallurgical*

Transactions B. 23 B (1992) 371384.

7. P.Maran, T. Sornakumar, T. Sundararajan, Modeling of linear gas tungsten arc welding of stainless steel, *Metallurgical and Materials Transactions B*, 39B, (2008) 619-628.
8. P. Maran, T. Sornakumar, T. Sundararajan, Numerical studies on convection in GTA weld pool, *Indian Welding Journal* 41 (2008) 42-47.
9. T. Iamboliev, S. Katayama, A. Matunawa, Interpretation of phase formation in austenitic stainless steel welds, *Welding Journal*. 82 (2003) 337-s-347-s.
10. B.Basu, R.Raman, Microstructural variations in a high strength structural steel weld under isoheat input conditions, *Welding Journal*. 81 (2002) 239-s to 249-s.
11. N.Inoue, T.Muroga, A.Nishimura, O. Motojima, Correlation between microstructure and hardness of a low activation ferritic steel (JLF-1) weld joint, *Journal of Nuclear Materials*. 258-263 (1998) 1248-1252.
12. A.F. Norman, V. Drazhner, P.B. Prangnell, Effect of welding parameters on the solidification microstructure of autogenous TIG welds in an Al-Cu-Mg-Mn alloy, *Materials Science and Engineering A*. 259 (1999) 53-64.

Table 1 Properties of AISI 304L stainless steel

Properties	Symbols	Values
Thermal Conductivity(solid)	ks	31.39 Wm ⁻¹ K ⁻¹
Thermal Conductivity(liquid)	kl	15.48 Wm ⁻¹ K ⁻¹
Convection heat transfer coefficient	h	20 Wm ⁻² K ⁻¹
Density	?	7200 kgm ⁻³
Specific Heat	Cp	753 Jkg ⁻¹ K ⁻¹
Latent Heat	?H	2.1E 9 Jm ⁻³
Solidus Temperature	Tsol	1523 K
Liquidus Temperature	Tliq	1723 K
Viscosity	μ	0.005 kgm ⁻¹ s ⁻¹
Coefficient of thermal expansion	β	10 ⁻⁴ K ⁻¹

Table 2 Comparison of theoretical and experimental weld bead dimensions

Run No.	Current, Ampere	Voltage, Volt	Speed, mm/s	Heat input, kJ/mm	Tmax, K	Vmax, m/s	Theoretical bead dimension, mm		Experimental bead dimension, mm	
							Depth	Width	Depth	Width
1.	120	14.0	5.00	0.336	2620.24	0.185	1.098	4.213	1.150	4.01
2.	120	14.0	2.66	0.632	2933.03	0.182	1.793	5.434	2.100	5.53

Table 3 Micro hardness distribution in the weld bead for 120A, 14 V and 2.66 mm/s

S. No.	Y-distance	Hardness, VHN at X - distance from the line of symmetry of weld pool						
		0 mm	0.5 mm	1 mm	1.5 mm	2 mm	2.5 mm	3 mm
1	4.35 mm (Top surface)	279	210	199	220	224	219	197a
2	4.15 mm	204	172	199	222	190	187	219a
3	3.95 mm	242	210	199	210	204	190	238 a
4	3.75 mm	236	216	202	240	217	205 a	
5	3.55 mm	211	212	215	212	215	211a	
6	3.35 mm	221	217	252	199	212	197a	
7	3.15 mm	238	186	227	207	208a	207	
8	2.95 mm	216	195	175	228a	195		
9	2.75 mm	187	203	210a	190	229		
10	2.55 mm	217a	238a	237	192			
11	2.35 mm	237	232	228				
12	2.15 mm	223	214					

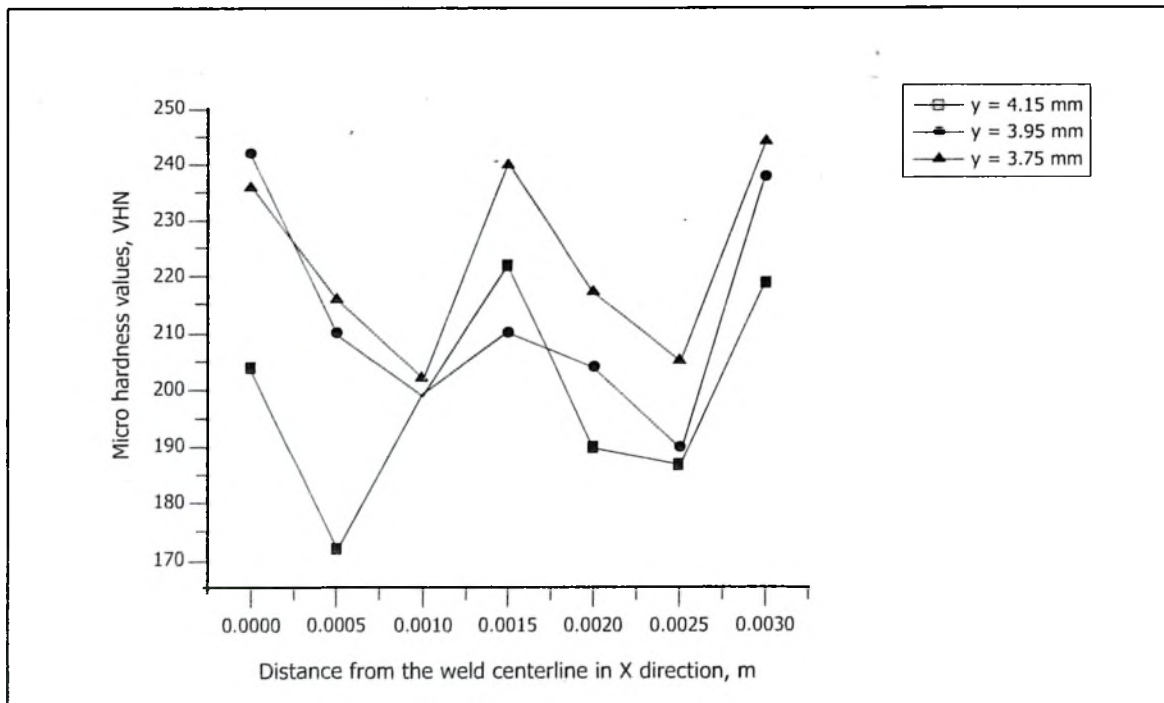


Fig. 1 Micro hardness variations in the weldment for 120A, 14V and 2.66 mm/s



Fig. 2 Microstructure in the unaffected zone

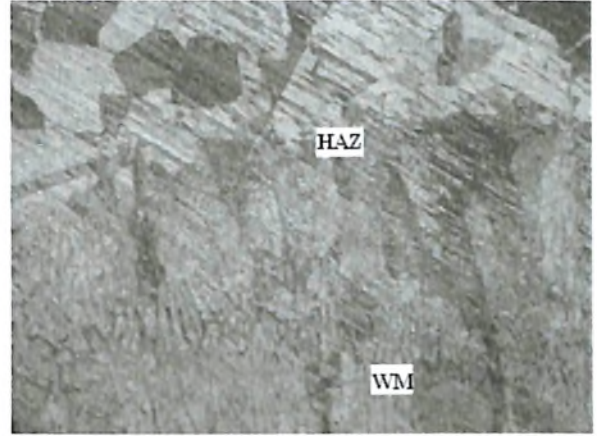


Fig. 3 Microstructure in the solid-liquid interface region for 120A, 14 V and 2.66 mm/s

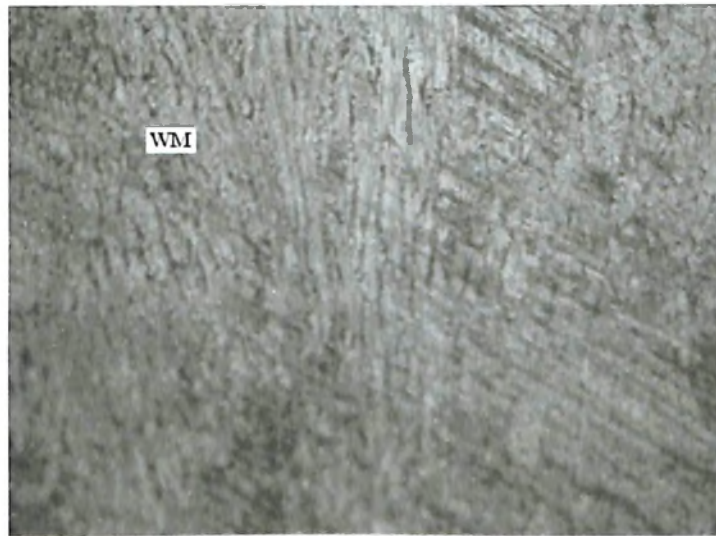


Fig. 4 Microstructure in the weld metal zone for 120A, 14 V and 2.66 mm/s